





Quantifying the Effect of Wind on Volcanic Plumes: Implications for Plume Modeling

Tobias Dürig¹ , Magnús T. Gudmundsson¹ , Fabio Dioguardi^{2,3} , and Louise Steffensen Schmidt⁴ 

¹Nordvulk, Institute of Earth Sciences, University of Iceland, Reykjavík, Iceland, ²British Geological Survey, The Lyell Centre, Edinburgh, UK, ³Now at University of Bari “Aldo Moro”, Dipartimento di Scienze della Terra e Geoambientali, Bari, Italy, ⁴Section of Physical geography and Hydrology, University of Oslo, Oslo, Norway

Key Points:

- Many wind-affected plume models require centerline heights H of bent-over plumes. We explore how to best obtain H from observations
- Observation-based strategies to convert top plume heights into centerline heights are presented and compared with theoretical approaches
- Results indicate optimal values of 0.28–0.36 for the wind entrainment coefficient in the Eyjafjallajökull 2010 eruption

Correspondence to:

T. Dürig,
tobi@hi.is

Citation:

Dürig, T., Gudmundsson, M. T., Dioguardi, F., & Schmidt, L. S. (2023). Quantifying the effect of wind on volcanic plumes: Implications for plume modeling. *Journal of Geophysical Research: Atmospheres*, 128, e2022JD037781. <https://doi.org/10.1029/2022JD037781>

Received 6 SEP 2022
Accepted 22 DEC 2022

Author Contributions:

Conceptualization: Tobias Dürig
Formal analysis: Tobias Dürig
Funding acquisition: Tobias Dürig
Investigation: Tobias Dürig
Methodology: Tobias Dürig
Project Administration: Tobias Dürig
Resources: Magnús T. Gudmundsson
Software: Louise Steffensen Schmidt
Validation: Tobias Dürig
Visualization: Tobias Dürig, Magnús T. Gudmundsson
Writing – original draft: Tobias Dürig
Writing – review & editing: Magnús T. Gudmundsson, Fabio Dioguardi, Louise Steffensen Schmidt

Abstract The considerable effects that wind can have on estimates of mass eruption rates (MERs) in explosive eruptions based on volcanic plume height are well known but difficult to quantify rigorously. Many explicitly wind-affected plume models have the additional difficulty that they require the use of centerline heights of bent-over plumes, a parameter not easily obtained directly from observational data. We tested two such models by using the time series of varying plume heights and windspeeds of the 2010 eruption. The mapped fallout and photos taken during this eruption allow us to estimate the plume geometry and to empirically constrain input parameters for the two models tested. Two strategies are presented to correct the difference in maximum plume height and centerline height: (a) based on plume radius, and (b) by using the plume type parameter Π , which quantifies the relative influence of buoyancy and cross-wind on the plume dynamics, to discriminate weak, intermediate and strong plumes. The results indicate that it may be more appropriate to classify plumes as either wind-dominated, intermediate or buoyancy-dominated, where the relative effects of both wind and MER define the type. The analysis of the Eyjafjallajökull data shows that the MER estimates from both models are considerably improved when a plume-type dependent centerline-correction is applied. For one model, we varied the wind entrainment coefficient β . For this particular eruption, we find that the best value for β lies between 0.28 and 0.36, unlike previous suggestions that set this parameter to 0.50.

Plain Language Summary When a volcano explosively erupts, hot magma fragments (called “ash”) are expelled into the atmosphere. Hot ash, gas and steam form mighty columns, which are called “ash plumes.” Ash in the air is dangerous for planes. For volcanologists it is therefore very important to estimate as quickly as possible how much of ash is pushed into the air. We cannot directly measure the amount, but there are mathematical equations (called “models”) that help us to estimate it. These equations require the top height of the plume as main input. If it is very windy, however, ash plumes are bent to the side, and we cannot simply use the top plume height as input anymore. Instead, we need to apply some correction, so that the model still can be used. Here, we present and examine such correction strategies. As test case, we use an Icelandic eruption that lasted 39 days and took place under different wind conditions.

1. Introduction

Explosive eruptions are characterized by the production of volcanic ash, which can be injected into the atmosphere by buoyant eruptive columns (e.g., Sparks et al., 1997; Wilson & Walker, 1987; Woods, 1988). Since ash can be harmful in several ways in modern society, for example, for aviation, infrastructure, agriculture, water supply, or human health (e.g., Blake et al., 2017; Blong et al., 2017; Giehl et al., 2017; Grindle & Burcham, 2002; Jenkins et al., 2015) monitoring eruptive plumes in real-time is an important task for prompt hazard mitigation. One of the key parameters required to predict the eruptive plume dynamics and the subsequent atmospheric dispersal of the erupted tephra is the mass eruption rate (MER), that is, the mass flux (kg s^{-1}) of tephra injected into the atmosphere (e.g., Bonadonna et al., 2016; Dioguardi et al., 2016; Mastin et al., 2009; Sparks et al., 1997; Wilson & Walker, 1987). Plume models of various degrees of complexity exist to estimate the current MER at the source based on the top plume height h (for overview see Costa et al., 2016), but only 0D and 1D models are at present fast enough to be applicable for mass flux assessment in real-time. The 0D models consist of a single equation linking MER to the top plume height based on empirical observations or theoretical considerations; the 1D-models solve the conservation of mass, momentum, and energy to obtain the plume trajectory, specifically the trajectory of a hypothetical plume centerline. Compared to 0D models, 1D models are more accurate but are

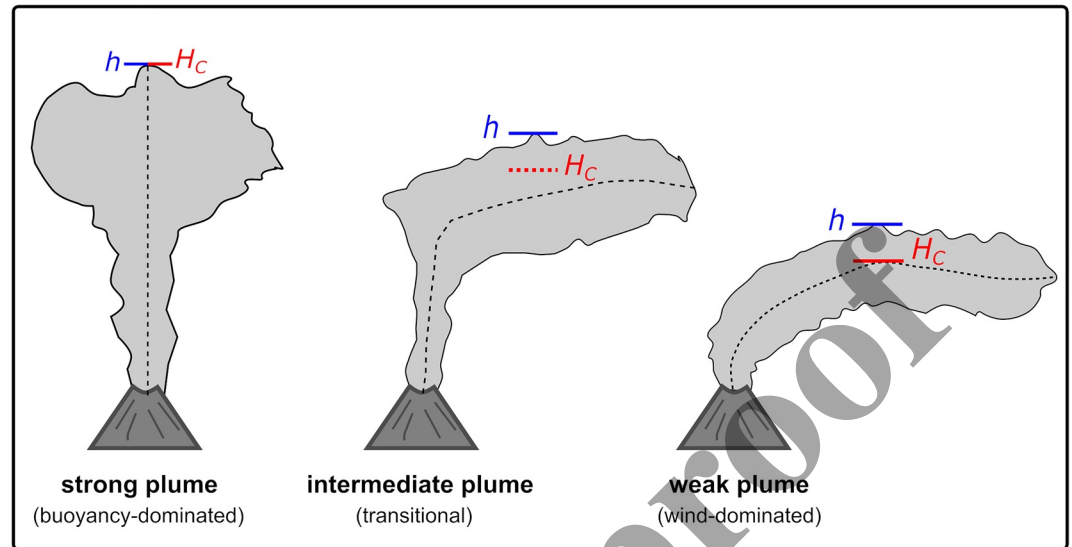


Figure 1. Illustration of plume types. “Strong plumes” are ash columns which rise vertically into the atmosphere. For this plume type, top plume height h (blue bar) and optimal model input height H_c (red bar) coincide. Centerlines are indicated by black dashed lines. A “weak plume” is bent-over, and strongly influenced by the horizontal wind field. In such a case, H_c coincides with the maximum centerline height and can be calculated by subtracting the plume radius from h . “Intermediate plumes” are settled between the two endmember conditions. For intermediate plumes H_c lies below h , but also above the maximum elevation of the centerline.

also more challenging to use in operational applications since they require more implicit assumptions of initial conditions that are usually not readily available in real-time (e.g., starting plume geometry at the vent, mass fraction of external water at source). The 0D and 1D plume models can be divided into two groups: (a) not explicitly wind-affected plume models (WAMs; e.g., Mastin et al., 2009; Sparks et al., 1997; Wilson & Walker, 1987; Woods, 1988); (b) explicitly WAMs, which take the atmospheric conditions at the eruption site into account (e.g., Bursik, 2001; de’Michieli Vitturi et al., 2015; Degruyter & Bonadonna, 2012; Devenish, 2013; Folch et al., 2016; Mastin, 2014; Woodhouse et al., 2013).

Since WAMs solve for the plume trajectory, which is defined at the centerline of the plume, they generally require the top elevation of the plume’s centerline H_c to calculate MERs. The optimal model input for H_c depends, however, on the plume type (Mastin, 2014), for which three cases are distinguished (Figure 1; see also Section 2.4). (a) “Strong plumes”: for vertically rising plumes in a weak wind field, the top plume height h can be used for H_c . (b) “Weak plumes”: for a wind-dominated horizontally distorted “bent-over” plume in a strong wind field, the plume radius has to be subtracted from h to obtain H_c , which coincides with the plume’s centerline at its maximum elevation. (c) “Intermediate plumes”: for transitional plumes, the modeled plume height H_c is larger than the centerline, but lower than the top plume height h . Any centerline-correction strategy thus has two crucial aspects: (a) the correction parameter itself (usually by using the plume radius), and (b) a definition of criteria used to decide on whether a correction is applied or not.

Solvers of 1D models employ various strategies to find the best approximation of H_c (Devenish, 2016; Folch et al., 2016; Mastin, 2014; Scollo et al., 2019). In contrast, applications of many 0D WAMs (e.g., Degruyter & Bonadonna, 2012; Woodhouse et al., 2013) suggested the usage of H_c as explicit input parameter (Dioguardi et al., 2020; Dürig, Gudmundsson, Ágústsdóttir, et al., 2022; Dürig et al., 2018; Londono & Galvis, 2018; Rossi et al., 2019). Any mismatch between H_c and h is expected to result in large discrepancies between models and empirical data, due to the strongly non-linear relationship between plume height and MER (Dürig, Gudmundsson, Ágústsdóttir, et al., 2022; Mastin, 2014). Therefore, the observed plume top height h has first to be converted to the model input height H_c , before plugging it into a 0D WAM.

Here, we explore observation-based centerline-correction approaches that enhance the ability of WAMs to provide accurate MER estimates. We introduce two strategies to utilize observational data of plume radii for converting top plume height data h into model input heights H_c , and test them with two 0D WAMs that do not include an

in-built centerline-correction: the models by Degruyter and Bonadonna (2012) and by Woodhouse et al. (2013), subsequently labeled “DBM” and “WM,” respectively. Both models are implemented in the real-time mass flux monitoring software REFIR (Dioguardi et al., 2020; Dürig et al., 2018). To constrain the parameters introduced, we use empirical data from the 2010 eruption of Eyjafjallajökull, Iceland, which featured distinct eruptive phases with predominantly weak and intermediate plumes. We explore the suitability of application criteria of centerline-corrections and compare the results from our observation-based strategies with the outcome of theoretical correction approaches for 1D WAMs, suggested by Devenish (2016) and Scollo et al. (2019). Finally, we discuss the potential implications of our findings for the optimal choice of centerline-correction strategy, correction factors and wind entrainment coefficient for the Eyjafjallajökull 2010 eruption. For definition of parameters and abbreviations used in this study, see Table 1.

2. Methods

2.1. The Eruptive Phases of Eyjafjallajökull 2010

The 2010 Eyjafjallajökull eruption was characterized by four distinctive main phases (phases I to IV, see Table 2). Phase I (14–18 April) was an initial explosive phase with phreatomagmatic activity (Dellino et al., 2012). The predominant wind direction on 14–16 April changed from westerly winds to northerly winds bending the plume to the south (Gudmundsson et al., 2012). As a result, the erupted mass could be determined for both sub-phases (labeled “Ia” and “Ib”). The subsequent phase II lasted 16.5 days (18 April–4 May) and was characterized by relatively low discharge with mixed effusive and explosive activity, followed by phase III (5–17 May) when effusive activity ceased with revived, more vigorous explosive activity. Often referred to as “the second explosive phase,” this phase showed pulsating activity linked to magmatic fragmentation (Dürig, Gudmundsson, & Dellino, 2015; Dürig, Gudmundsson, Karmann, et al., 2015; Ripepe et al., 2013). With declining explosive activity, phase IV (18–22 May) concluded the eruption. The ash plume top fell below the radar detection limit of 2.5 km on 21 May, 10:20 UTC, and remained below it until the end in late 22 May (Arason et al., 2011). The eruption's fallout was measured at about 400 locations in Iceland, including good coverage in the proximal area, leading to the mass estimates M_{ground} with uncertainties listed in Table 2. For the methodology applied and details on the estimation of mass uncertainties, see Gudmundsson et al. (2012) and Dürig, Gudmundsson, Ágústsdóttir, et al. (2022).

2.2. Radar Records and Weather Reanalysis Data

The top plume heights h used in this study are based on records obtained by a C-band radar station in Keflavík (Arason et al., 2011), about 150 km to the WNW of Eyjafjallajökull (Figure 2). A recent study calibrated the radar data by comparing the radar plume heights with those measured in photographs taken throughout the eruption (Dürig, Gudmundsson, Ágústsdóttir, et al., 2022). It found that radar heights underestimated the top plume heights by on average 0.5 km. Therefore, we corrected the plume height data accordingly.

Reanalysis of data from the ERA5 and HARMONIE-AROME (ICRA) were used to obtain the atmospheric parameters. While ERA5 is a global reanalysis data set with a horizontal resolution of 30 km over Iceland (Hersbach et al., 2018, 2020), ICRA is a local reanalysis product from the Icelandic Met Office with a horizontal resolution of 2.5 km, based on the non-hydrostatic numeric weather prediction model HARMONIE-AROME (Nawri et al., 2017; Schmidt et al., 2018). In ERA5, the atmosphere is described by 137 vertical pressure levels with a top layer at 80 km above ground level in 1 hr intervals (a.g.l.), whereas HARMONIE-AROME resolves the atmosphere in 65 levels up to 30 km a.g.l. The data are archived at four pressure levels in ICRA: 500, 850, 925, and 1,000 hPa in 1 hr intervals (Nawri et al., 2017). Windspeeds from both data sets were linearly interpolated to 5 min intervals.

2.3. Plume Models Tested

The first of the two tested WAMs (DBM) was developed by Degruyter and Bonadonna (2012) and is based on a combination of the buoyant plume theory of Morton et al. (1956) and its modification by Hewett et al. (1971) to take the effect of cross-flow (e.g., wind) into account. It computes the mass flux by:

$$\text{MER}_{\text{DBM}} = \pi \frac{\rho_{a0}}{g'} \left(\frac{2^{5/2} \alpha^2 \bar{N}^3}{z_1^4} H_C^4 + \frac{\beta^2 \bar{N}^2 \bar{V}}{6} H_C^3 \right) \quad (1)$$

Table 1
Abbreviations and Parameters

Term	Description	Units
<i>Abbreviations</i>		
WAM	Wind-affected plume model	
DBM	Plume model by Degruyter and Bonadonna (2012)	
WM	Plume model by Woodhouse et al. (2013)	
MER	Mass eruption rate	kg/s
<i>Parameters</i>		
h	Maximum height of the plume top	km
H_c	Maximum height of a weak plume's centerline	km
ρ_{a0}	Atmospheric density at volcanic source	kg m ⁻³
α	Radial entrainment coefficient	–
β	Wind entrainment coefficient	–
\bar{V}	Plume height-averaged windspeed	m s ⁻¹
V_1	Windspeed at reference height H_1	m s ⁻¹
\bar{N}	Plume height-averaged buoyancy frequency	s ⁻¹
T_a	Atmospheric temperature	K
T_{a0}	Atmospheric temperature at volcanic source	K
T_0	Magmatic temperature at the source	K
C_{a0}	Heat capacity of atmosphere at volcanic source	J K ⁻¹
C_0	Heat capacity of magma at the source	J K ⁻¹
g	Gravitational acceleration	m s ⁻²
g'	Reduced gravity	m s ⁻²
\bar{W}_s	Wind shear from ground to reference height H_1	–
MER _{model}	Predicted mass eruption rate, according to selected model	kg s ⁻¹
M_{model}	Predicted erupted mass of tephra, according to selected model	kg
M_{ground}	Observed erupted mass of tephra	kg
Π	Plume classification parameter	–
Π_l	Lower plume classification threshold	–
Π_u	Upper plume classification threshold	–
$\hat{\nu}$	Dimensionless windspeed	–
$\bar{\nu}$	Dimensionless windspeed	–
γ	Average wind shear	s ⁻¹
F'_{BO}	Effective buoyancy of the plume	m ⁴ s ⁻³
r_{model}	Modeled plume radius, normalized to top plume height h	–
r_{obs}	Observed plume radius, normalized to top plume height h	–
D	Plume diameter at maximum plume height	m
a	Plume height correction factor for intermediate plumes	–
b	Plume height correction factor for wind-affected (“weak”) plumes	–

Here and in the following, ρ_{a0} is density; the subscripts a and 0 refer respectively to the atmosphere and volcanic source vent height. α and β are respectively the radial and wind entrainment coefficients, and \bar{V} is the plume height-averaged windspeed. H_c refers to the plume's maximum centerline height above the vent (exceptions will be discussed below), $z_1 = 2.8$ is the maximum non-dimensional height resulting from numerical integration of the governing equations of Morton et al. (1956), g' is reduced gravity (see below). The buoyancy

Table 2
Phases of the 2010 Eyjafjallajökull Eruption^a

Phase	Date	Duration (min)	M_{ground} ($\times 10^{10}$ kg)	$\text{MER}_{\text{ground}}$ ($\times 10^5$ kg/s)	Time-averaged windspeed m/s	Strong (%)	Interm. (%)	Weak (%)
Ia	14/04–16/04	3,785	9.8 ± 2.1	4.3 ± 0.9	36.4	0.0	5.5	94.5
Ib	17/04–18/04	2,165	3.5 ± 1.0	2.7 ± 0.8	19.2	0.0	38.0	62.0
I (total)	14/04–18/04	5,945	13.3 ± 3.0	3.7 ± 0.9	30.1	0.0	18.1	81.9
II	18/04–04/05	23,765	4.2 ± 1.4	0.3 ± 0.1	11.8	1.2	53.1	45.7
III	05/05–17/05	18,725	18.9 ± 4.9	1.7 ± 0.4	16.2	1.3	40.1	58.6
IV	18/05–21/05	4,950	1.4 ± 0.4	0.5 ± 0.1	14.5	0.0	15.7	84.3
All	14/04–21/05	53,385	37.8 ± 9.8	1.2 ± 0.3	15.6	1.0	39.6	59.4

^aThe estimated erupted airborne tephra mass M_{ground} is from Gudmundsson et al. (2012). Dividing M_{ground} with duration results in the average mass eruption rate $\text{MER}_{\text{ground}}$. The three last columns show the percentage of duration, for which the plume was classified as strong ($\Pi > 0.5$, see also Figure 1), weak ($\Pi < 0.1$) or intermediate ($0.1 = \Pi \leq 0.5$). In addition, time-averaged windspeeds are given for each phase.

frequency at height z above source is N while the parameter used is \overline{N} , the height-averaged value, calculated as:

$$\overline{N}^2 = \frac{1}{H_C} \int_0^{H_C} N^2(z) dz = \frac{1}{H_C} \frac{g}{C_{a0} T_{a0}} \int_0^{H_C} \left(1 + \frac{C_{a0}}{g} \frac{dT_a}{dz} \right) dz \quad (2)$$

where g is the gravitational acceleration, T is the temperature, and C is the heat capacity. In Equation 1, the reduced gravity at the source g' is defined as:

$$g' = g \frac{C_0 T_0 - C_{a0} T_{a0}}{C_{a0} T_{a0}} \quad (3)$$

We used a specific heat capacity C_0 of $1,250 \text{ J kg}^{-1} \text{ K}^{-1}$ for the ash, $998 \text{ J kg}^{-1} \text{ K}^{-1}$ for the atmosphere, and of $1,624 \text{ J kg}^{-1} \text{ K}^{-1}$ for the mixture at the vent, in accordance with the parameters used by Degruyter and Bonadonna (2012) and Woodhouse et al. (2013), respectively. As source temperature we used 1323 K, which lies in the range of 1298–1336 K found by means of plagioclase-clinopyroxene geothermometry for Eyjafjallajökull 2010 (Keiding & Sigmarrsson, 2012). The second plume model tested (Woodhouse et al., 2013) is based on a relationship between MER and plume height from a numerical 1D model using $\beta = 0.9$. Thus, unlike the DBM, β is not adjustable in the 0D formulation of this model. The WM calculates the mass flux by:

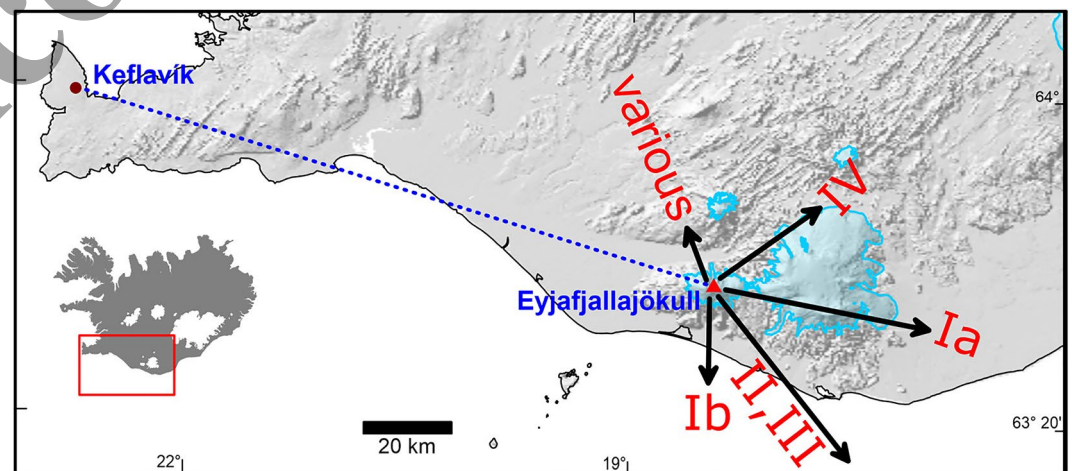


Figure 2. Location of Eyjafjallajökull. The plume heights of the 2010 eruption were recorded by a C-band radar stationed at Keflavík airport, approximately 150 km from the volcano. Major axes of tephra dispersion are indicated by arrows, labels indicate the dominant direction for each phase (for details, see Gudmundsson et al., 2012).

$$\text{MER}_{\text{WM}} = \left(\frac{1}{0.318} H_c \frac{1 + 4.266\tilde{W}_s + 0.3527\tilde{W}_s^2}{1 + 1.373\tilde{W}_s} \right)^{3.953} \quad (4)$$

where the parameter \tilde{W}_s describes the wind shear from the ground to a reference height H_1 according to:

$$\tilde{W}_s = 1.44W_s = 1.44 \frac{V_1}{N H_1} \quad (5)$$

with V_1 being the windspeed at a reference height H_1 that coincides with H_c (Woodhouse et al., 2013).

For DBM and WM, input parameters (h , V_1 , and \bar{V}) were assessed by progressing in steps of 5 min and calculating the 3 hr moving average. This procedure is described as “dynamic plume height and MER reconstruction strategy” and was found to be advantageous for WAMs (Dürig, Gudmundsson, Ágústsdóttir, et al., 2022). For each eruptive phase, the MER was estimated with each of the two models. The total mass M_{model} was determined by integrating the resulting MERs over the eruption time.

Like most 0D and 1D plume models, DBM and WM assume that the plume is fed by a continuous stream of ash and gas. The Eyjafjallajökull 2010 eruption showed pulsating behavior, which theoretically violates the models' assumption of steadiness. However, using a time-dependent pulse velocity-derived model (Dürig, Gudmundsson, Karmann, et al., 2015; Hochfeld et al., 2022), a study found that the pulse frequency was high enough to treat the Eyjafjallajökull plume as a steady plume (Dürig, Gudmundsson, Karmann, et al., 2015).

2.4. Plume Type Classification

If the vertical rise rate of a buoyant ash plume is much greater than the horizontal windspeed, it cuts through the horizontal wind field and forms a vertical column. Such a plume is referred to as being “strong,” according to standard volcanological terminology (Carey & Sparks, 1986; Mastin, 2014). For this type of plumes, H_c and h are equal (Figure 1). Conversely, a bent-over plume, where the vertical rise rate is similar to, or smaller than the horizontal windspeed, forms the other endmember of plume types and is classified as “weak.” For these plumes, the maximum centerline height H_c can be obtained by subtracting the plume radius from h (Mastin, 2014). Plumes that group between the two endmembers are denoted “intermediate.” For intermediate plumes, finding the correct value for H_c is challenging, since a distance smaller than the actual plume radius has to be subtracted to achieve a correct MER estimate (Devenish, 2016; Mastin, 2014). We note that in these cases, H_c is *not* the maximum height of the centerline, but a reconstructed height that represents the optimal model input (see Section 2.5.2).

In order to classify the plumes, we used the scaled parameter Π , which quantifies the relative influence of buoyancy and cross-wind on the plume dynamics and is defined as (Degruyter & Bonadonna, 2012):

$$\Pi = \frac{\bar{N}h}{1.8 \cdot \bar{V}} \cdot \left(\frac{\alpha}{\beta} \right)^2 \quad (6)$$

in combination with two classification thresholds Π_l and Π_u . A strong plume is indicated by large values for Π ($\Pi > \Pi_u$), a weak plume by very low values ($\Pi < \Pi_l$) and a value between these thresholds ($\Pi_l \leq \Pi \leq \Pi_u$) indicates a plume of intermediate type (Bonadonna et al., 2015). Originally, it was suggested that Π_l and Π_u are 0.1 and 10, respectively, but a more recent study revised the upper threshold Π_u to be 0.5, based on photogrammetric measurements of paroxysms at Etna (Scollo et al., 2019).

For Eyjafjallajökull 2010, Π was calculated by using the top plume height data and the software REFIR (Dürig et al., 2018). To be consistent with the approach of Scollo et al. (2019), we used for all computations of Π a radial entrainment coefficient of $\alpha = 0.1$ and a wind entrainment coefficient $\beta = 0.5$.

In order to test if Π_l and Π_u found by Scollo et al. (2019) for Etna can serve as “global” thresholds, we also computed Π for a set of 25 eruptions, in the following referred to as the “Mastin data set,” using the times, geographical location and plume heights provided by Mastin (2014), and ERA5 reanalysis data. For these eruptions, Mastin (2014) presented dimensionless windspeeds \hat{v} and \hat{v} , calculated by:

$$\hat{v} = \frac{\gamma}{N} \quad (7)$$

with γ being the average wind shear (in s^{-1}), and:

$$\bar{v} = \frac{\bar{V}}{(F'_{\text{BO}} \cdot \bar{N})^{0.25}} \quad (8)$$

with F'_{BO} being the plume's effective buoyancy flux at the vent (Mastin, 2014). According to the findings of that study, weak plumes are characterized by \hat{v} values larger than 0.35 and \bar{v} values larger than 1. Conversely, for strong plumes \hat{v} and \bar{v} was found to be much smaller than 0.35 or 1, respectively.

2.5. Converting Recorded Plume Heights h Into Model Input Heights H_C

Using h instead of H_C as input for the WAMs might often result in an overestimation of the MER (Mastin, 2014). For example, for the complete eruption of Eyjafjallajökull 2010, the erupted mass computed by WM is more than 70% larger than M_{ground} (Dürrig, Gudmundsson, Ágústsdóttir, et al., 2022). As discussed above, this inconsistency arises in cases where the plume is deflected by wind as opposed to rising vertically; the centerline can be located considerably below the plume top (Figure 1). In this study, we explore several approaches to convert the observational data (i.e., top plume height h , plume radius, and Π) into model input heights H_C .

2.5.1. Simple Radius Subtraction Approach (“ r -Strategy”)

In the r -strategy, the observed plume radius is used to compute H_C , regardless of the plume type. H_C is calculated by:

$$H_C = h \cdot (1 - r) \quad (9)$$

where the parameter r represents the plume radius normalized to h . For the 2010 Eyjafjallajökull eruption, we computed the solutions for H_C and r , for which the modeled mass M_{model} lies within the uncertainty range of M_{ground} (Table 2).

To find out how these results fit with the observations, we compared the solutions for r with actual observations of plume radii. For this purpose, we browsed through a very large data set of hundreds of photos depicting the ash plume taken from aircraft during inspections flights (Dürrig, Gudmundsson, Ágústsdóttir, et al., 2022), and we determined the plume diameters at the top of the plume's trajectory by means of photogrammetric measurements with the Python software Pixelcalc (Magnússon, 2012). To ascertain the maximum measurement accuracy we selected photos taken in the air (a) at a known time and (b) known coordinates, (c) featuring a weak bent-over plume ($\Pi < \Pi_c$) (d) from an angle perpendicular to the plume allowing measurement of the plume diameter without optical distortion effects (Dürrig, Gudmundsson, Ágústsdóttir, et al., 2022; Scollo et al., 2014) (e) showing the vent or a cloud cover of known elevation, suitable as reference level. From the several hundred photos inspected, 31 images from 13 days fulfilled all five criteria.

2.5.2. Plume Type-Dependent Model Input Tuning Approach (“ ab -Strategy”)

As a refinement of the r -strategy, the ab -strategy was developed to constrain H_C by distinguishing the plume conditions using the plume-type indicator Π .

Two plume-type specific correction factors (a and b) were introduced with $a \geq b$, that convert top plume heights h into model input heights H_C according to:

$$H_C = h; \text{ if } \Pi > \Pi_u; \text{ (“strong plume”)} \quad (10)$$

$$H_C = h \cdot (1 - b); \text{ if } \Pi_l \leq \Pi \leq \Pi_u; \text{ (“intermediate plume”)} \quad (11)$$

$$H_C = h \cdot (1 - a); \text{ if } \Pi < \Pi_l; \text{ (“weak plume”)} \quad (12)$$

The parameter a can be seen as the radius of a weak plume, normalized with respect to h . The normalized correction factor required to obtain the optimal model input H_C from the top plume height h for intermediate plumes is given by the parameter b . Using intervals of 5 min, for each eruptive phase and model, the MER was assessed by feeding the models with H_C , which was computed according to the respective Π -values. The resulting MER estimates were multiplied by 300 s and cumulatively summed over the period analyzed, resulting in M_{model} . The

parameters a and b were varied between 0 and 0.9 with a step-size of 0.01. Then, for each combination of a and b the differences between the mean values of measured mass M_{ground} and modeled masses M_{model} were computed and normalized with respect to M_{ground} . We then determined the values of a and b which provided the best fit between model and observations.

2.5.3. Theoretical Centerline-Corrections

A plume theory-based correction strategy introduced by Devenish (2016) computes H_c with:

$$H_C = h \cdot (1 - r_{\text{Dev}}); \text{ if } \bar{v} > 1 \quad (13)$$

where the radius normalized to top plume-height r_{Dev} is predicted with:

$$r_{\text{Dev}} = \frac{\beta}{(1 + \beta)} \quad (14)$$

While the approach by Devenish (2016) applies the centerline-correction for $\bar{v} > 1$, Scollo et al. (2019) modified Equation 13 by using a threshold of $\Pi < 0.1$, instead. The two approaches are subsequently called “Devenish-strategy” and “Scollo-strategy.”

3. Results

3.1. Findings for Plume-Type Indicator Π

The results of the computations of Π for the 25 eruptions of the Mastin data set are shown in Figure 3a with the Π values for each phase of the 2010 eruption of Eyjafjallajökull displayed. Vertical dashed lines mark the thresholds $\Pi_l = 0.1$ and $\Pi_u = 0.5$ as suggested by Scollo et al. (2019). According to this Π -based classification scheme, the majority of plumes from the Mastin data set are classified as strong or intermediate, and only five of them fall into the group of weak plumes. The latter are displayed as red circles in Figure 3b, where the dimensionless windspeeds \bar{v} and \hat{v} reported in Mastin (2014) are plotted against each other. Following the dimensionless windspeeds-based plume-type classification scheme by Mastin (2014), weak plumes are characterized by a \bar{v} larger than 1 and a \hat{v} larger than 0.35 (indicated by dashed lines in Figure 3b). Four of the five plumes classified as “weak” with the Π -based classification scheme fulfill also at least one of the two criteria for weak plumes according to the dimensionless windspeed-based classification scheme. The only exception is the plume of Mt. St. Helens from 12 June 1980 (“Mt St Helens 1980/3”), with a \bar{v} of 0.96, a \hat{v} of 0.31 (suggesting it to be intermediate) and an average Π of 0.097 (suggesting it to be weak, see also Figure 3a). Despite these seemingly conflicting plume-type assignments for this particular plume, both classification schemes agree in characterizing it as marginal, by placing it at the border between the two plume-types. Our comparison therefore confirms to a large part the findings of Bonadonna et al. (2015) and Scollo et al. (2019): using a lower threshold of $\Pi_l = 0.1$ leads to a reasonable distinction between weak and intermediate plumes. Since intermediate and strong plumes overlap in the \bar{v} versus \hat{v} diagram (Figure 3b), it is not possible to test the global validity of Π_u in a similar way, but based on our findings on the eruptions from the Mastin data set (Figure 3a), an upper threshold of $\Pi_u = 0.5$, as found by Scollo et al. (2019) appears to be more plausible than the originally suggested threshold Π -value of 10 (Bonadonna et al., 2015), for which none of the 25 eruptions would qualify as “strong.” Subsequently, we therefore use $\Pi_l = 0.1$ and $\Pi_u = 0.5$ as lower and upper thresholds, respectively.

Figure 4 shows the temporal evolution of Π during the Eyjafjallajökull 2010 eruption. To test the potential differences arising from the choice of the atmospheric model, we computed Π with atmospheric data parameters retrieved from the ERA5 data set (blue curve) and the HARMONIE-AROME data (black curve). The differences between the two Π curves are relatively small. This is even more evident for the Π -values averaged over each of the four main eruptive phases (horizontal dashed lines). In both time series the plume was weak in phase I and IV, and intermediate in phases II and III. This finding agrees well with the results of Dürig, Gudmundsson, Ágústsdóttir, et al. (2022), that for the Eyjafjallajökull 2010 eruption the effect of the choice of atmospheric model on the modeled MER is small compared to the model uncertainties. In the following, we therefore focus on the results obtained with reanalysis data from ERA5.

Based on the Π -values displayed in Figure 4, we also binned the plume-type in 5-min intervals and quantified the percentages of bins of each plume-type for each eruption phase and for the whole eruption (Table 2). It was

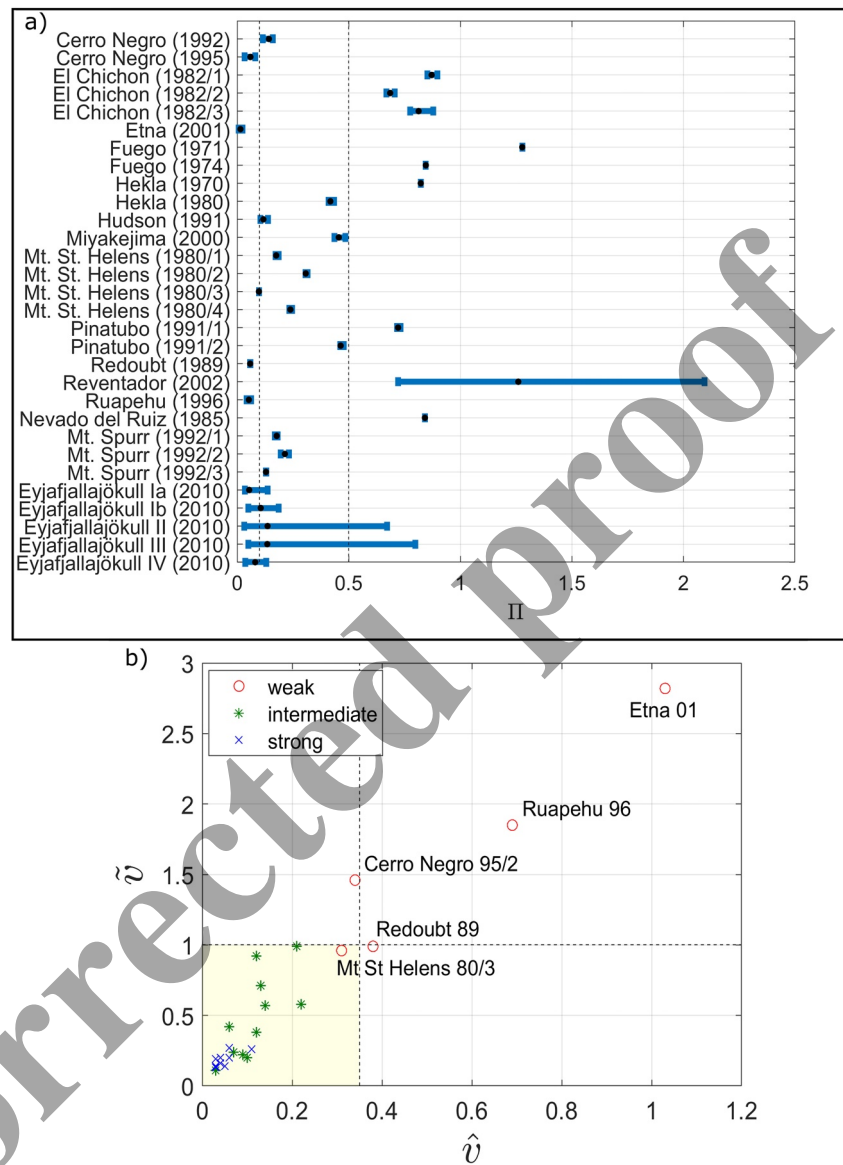


Figure 3. Comparison of plume type classification schemes. (a) Π -ranges for 25 eruptions, computed by Equation 6 with plume height data from Mastin (2014) and ERA5 reanalysis data. Mean values are indicated by black markers. The thresholds $\Pi_l = 0.1$ and $\Pi_u = 0.5$ suggested by Scollo et al. (2019) are indicated by vertical dashed lines. They separate the three plume types (“weak,” “intermediate,” and “strong”). In addition, the ranges of Π are displayed for each eruptive phase of Eyjafjallajökull 2010. Note that for the computation of the latter, plume height data of much higher temporal resolution was used. (b) For 25 eruptions the dimensionless windspeeds \hat{v} and \hat{v} are plotted against each other, based Mastin (2014). Each eruption is represented by a data point. Symbol and color of each data point indicates plume-type according to Π . Eruptions that were classified as “weak” according to the Π classification scheme are labeled. According to Mastin (2014) a weak eruption is characterized by \hat{v} larger than 1, and \hat{v} larger than 0.35 (indicated by dashed lines). According to this classification scheme, strong plumes are grouped in the area marked in yellow.

found that the plume was predominantly weak (for ~59% of the total eruption time) or intermediate (for ~40% of the total eruption time), and only very sporadically fulfilling the conditions of a strong plume (~1% of the total eruption time). Interestingly, this approach results in a classification of the plume in phase III as weak most of the time (58.6%), in contradiction to what the phase-averaged Π suggests (Figure 4). The large values of Π at the end of phase III skew the phase-average to higher values, “pushing” it over Π_l . This example demonstrates the importance of time scale and methodology for classifying plume-types and advises caution when comparing time series of high resolution with estimates based on a single plume height value (Figure 3a).

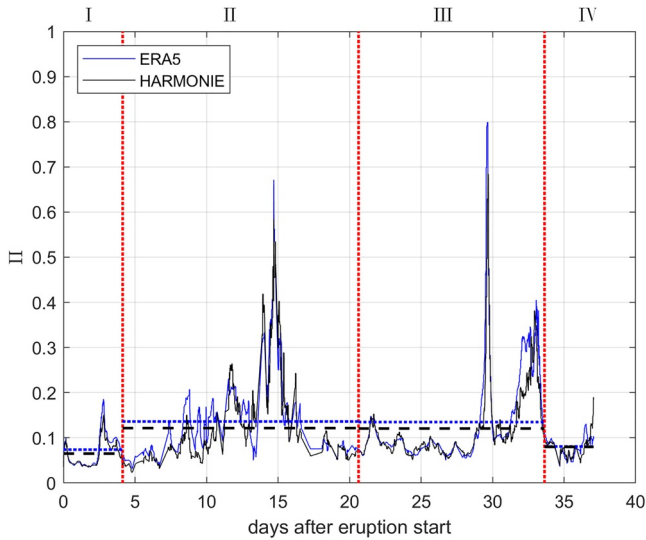


Figure 4. Π -values for the 2010 Eyjafjallajökull eruption. The bulk of this eruption was characterized by a weak ($\Pi < 0.1$) or intermediate ($0.1 = \Pi \leq 0.5$) plume. Vertical red lines separate the main eruptive phases. Horizontal dashed lines indicate the phase-averaged Π values.

uncertainty into plume models. The impact of the choice of β on the DBM is demonstrated in Table 3, where results for r_{DBM} with $\beta = 0.33$ and 0.5 are presented. Reducing β means that the efficiency of entrainment of the wind's horizontal momentum into the plume is decreased. As a consequence, for a given MER and windspeed the modeled plume will bend less, which means that the distance between H_c and h is reduced, resulting in a decrease of r_{DBM} . In other words, one has to subtract less from h , to obtain input data H_c that provide DBM predictions fitting with M_{ground} .

To examine which of the normalized plume radii r are plausible, we compare them with observations, based on the 31 photos that fulfill the selection criteria (see Section 2.5.1). Photos of the plume taken from different angles indicate that its cross-section can be approximated as cylindrical. The plume diameters D were photogrammetrically determined at 10 locations around the region of highest elevation (Figure 5a) and subsequently normalized with h . Assuming an accuracy of 0.5 km for h (Dürig, Gudmundsson, Ágústsdóttir, et al., 2022) and a measurement uncertainty of 200 m for the plume diameter D results for a 5 km high plume in an uncertainty for r_{obs} of only 1%, which is negligible compared to the typical variation of D around the region of interest. We therefore use the mean value as best estimate for r_{obs} , and the standard deviations of the 10 measurements as uncertainties. For days where several photos were available, the uncertainty of the diameter dD was estimated according to the law of error propagation by $dD = \sqrt{\sum_i (dD_i)^2}$, using the standard deviations dD_i measured for each photo. The observed normalized plume radius $r_{\text{obs}} = D/2h$ should for weak plumes with $\Pi < 0.1$ be identical to r in Equation 9. Table 3 presents the phase-averaged results for r_{obs} . In Figure 5b, the day-averaged values for r_{obs} are shown (black markers) and put into context with the predicted ranges for r_{WM} (blue areas), r_{DBM} with $\beta = 0.50$ (green areas) and r_{DBM} with $\beta = 0.33$ (red areas).

Although the 31 photos give only sporadic snapshots of a highly dynamic plume lasting for 39 days, the comparison in Figure 5b gives us some inferences. Using $\beta = 0.5$, no observed case r_{obs} falls within (or even close to) the predicted range r_{DBM} . Therefore, we infer that for all phases Eyjafjallajökull 2010 such a β -value is too high to reconstruct the MER with the DBM. In fact, the predictions r_{DBM} fit best with the observations r_{obs} for β ranging from 0.24 to 0.37, and with 0.33 when considering the total eruption (Table 3). The estimates by the WM r_{WM} correspond to the observations r_{obs} for the phases Ia, II, and IV (Figure 5b), as well as for the ranges of r_{obs} averaged over the total eruption ("all" in Table 3). However, according to our findings on r_{obs} , the WM requires considerably smaller values for r than r_{obs} to deliver a correct MER for phase Ib and -to a smaller degree- for phase III.

3.2. Outcomes From r -Strategy

Applying the r -strategy according to Equation 9 to the WM until $M_{\text{model}} = M_{\text{ground}}$ resulted in normalized plume radii listed as r_{WM} in Table 3. The normalized radii range from 0% to 12% (phase Ib) to a range of 19%–31% (phase II). Interestingly, the phases of low MER (phases II and IV, see Table 2) show the highest values for r_{WM} , regardless of the percentage of time when the plume was classified as weak (II: 45.7% vs. IV: 84.3%). This indicates that, compared to II, r_{WM} is less affected by windspeeds and more by MER. In contrast to the WM, the DBM requires the explicit predefinition of the radial and wind entrainment coefficients. The radial entrainment coefficient of volcanic plumes α is relatively well constrained to be ~ 0.1 from theoretical considerations (e.g., Carazzo et al., 2006; Degruyter & Bonadonna, 2012; Papanicolaou et al., 2008; Turner, 1986) and large-scale experiments with heated ash (Dellino et al., 2014). In addition, the r -strategy is very insensitive to variations in α : even when modeling the complete eruption using an unrealistically high α of 0.2, r_{DBM} would increase by less than 3%. The wind entrainment coefficient is, however, less well constrained. While studies using water tank experiments to examine the mixing of two fluids found $0.4 < \beta < 0.7$, with entrainment rates clustering around 0.5 (Contini et al., 2011; Huq & Stewart, 1996; Michaud-Dubuy et al., 2020), other studies suggested to use values for β ranging from 0.1 to 1.0 (e.g., Bursik, 2001; Suzuki & Koyaguchi, 2015; Woodhouse et al., 2013). This large range introduces an important source of

Table 3
Resulting Normalized Plume Radii r and Correction Factors a , b^a

	Row		Phase Ia	Phase Ib	Phase II	Phase III	Phase IV	All
<i>r</i> -Strategy	1	r_{WM} (%)	12–20	0–12	19–31	7–18	14–26	10–20
	2	r_{DBM} (%) $\beta = 0.50$	33–43	29–40	43–54	29–39	42–51	33–41
	3	r_{DBM} (%) $\beta = 0.33$	13–23	9–23	27–41	9–22	24–37	14–26
	4	r_{obs} (%)	16–21	15–24	20–31	16–26	13–22	18–25
	5	β	0.32	0.34	0.26	0.37	0.24	0.33
	6	r_{DBM} (%)	11–22	11–25	18–33	15–27	10–25	14–26
<i>ab</i> -Strategy	7	a_{WM} (%)	13–22	1–90	18–90	7–90	14–31	10–41
	8	b_{WM} (%)	0–20	0–13	3–31	0–17	0–22	0–20
	9	a_{DBM} (%) $\beta = 0.28$	4–16	3–71	19–90	0–33	15–35	5–33
	10	b_{DBM} (%) $\beta = 0.28$		0–18	5–31	0–13	0–22	0–19
	11	a_{DBM} (%) $\beta = 0.36$	17–28	15–90	30–90	13–90	27–48	17–63
	12	b_{DBM} (%) $\beta = 0.36$	0–20	8–24	27–31	0–25		5–24
	13	a_{DBM} (%) $\beta = 0.40$	22–33	20–90	34–90	18–90	31–54	22–90
	14	a_{DBM} (%) $\beta = 0.50$	33–43	30–90	42–90	28–90	40–69	32–90

^aThe ranges for r_{WM} and r_{DBM} (rows 1 and 2) quantify the normalized radii, for which, according to the *r*-strategy with Equation 9, the plume models WM (Woodhouse et al., 2013) and DBM (Degruyter & Bonadonna, 2012) deliver M_{model} that coincide with the fallout mass M_{ground} from the 2010 Eyjafjallajökull eruption. The DBM output depends on the selected wind entrainment coefficient β . Here, r_{DBM} results are given for $\beta = 0.5$ and $\beta = 0.33$. Row 4 shows the normalized observed plume radii r_{obs} under weak conditions ($\Pi < 0.1$). The range of r_{obs} for the complete eruption period (“all”) is calculated from the standard deviation of the measurements. In row 5 “optimal” values for β are presented, for which r_{DBM} (shown in row 6) correspond best to r_{obs} . Rows 7–14 shows the theoretically possible ranges for the correction factors a_{WM} and a_{DBM} when applying the *ab*-strategy to the models WM and DBM with the given wind entrainment coefficients β . Additionally, for each model the ranges of b consistent with $a = r_{obs}$ and modeled mass $M_{model} = M_{ground}$ are presented. An empty cell indicates that no solution exists.

3.3. Findings From *ab*-Strategy

In contrast to the *r*-strategy, the *ab*-strategy aims to use values of H_c with plume-type specific correction factors a and b , according to Equations 10–12. While a is applied to weak plumes and identical to the plume’s normalized radius, the correction factor b is applied for intermediate plumes. To test the *ab*-strategy, we calculated the resulting values for H_c under variation of all possible combinations of a and b and then used H_c as input for the models WM and DBM. The relative differences between modeled mass M_{model} and measured mass M_{ground} are presented in color maps in Figure 6. There, each pixel represents a pair of correction factors (a , b). A pixel corresponding to a pair (a , b) that leads to $M_{model} = M_{ground}$ has a dark blue color. The brighter the color of the pixel, the larger the relative difference of the modeled mass from what was measured. The dark blue pixels form a “corridor” of “possible” factor pairs (a , b) that lead to an accurate MER prediction.

For example, for 94.5% of the time, the plume in phase Ia was weak according to Π (Table 2). Therefore, the most relevant correction factor in this phase is a , while b plays no significant role. Consequently, the optimal “(a , b) corridor” forms a vertical line (Figure 6a). Conversely, the plume for phase II was for long periods of intermediate type. In such a case, the correct selection of b is dependent on a , reflected in a “tilted” “(a , b) corridor”

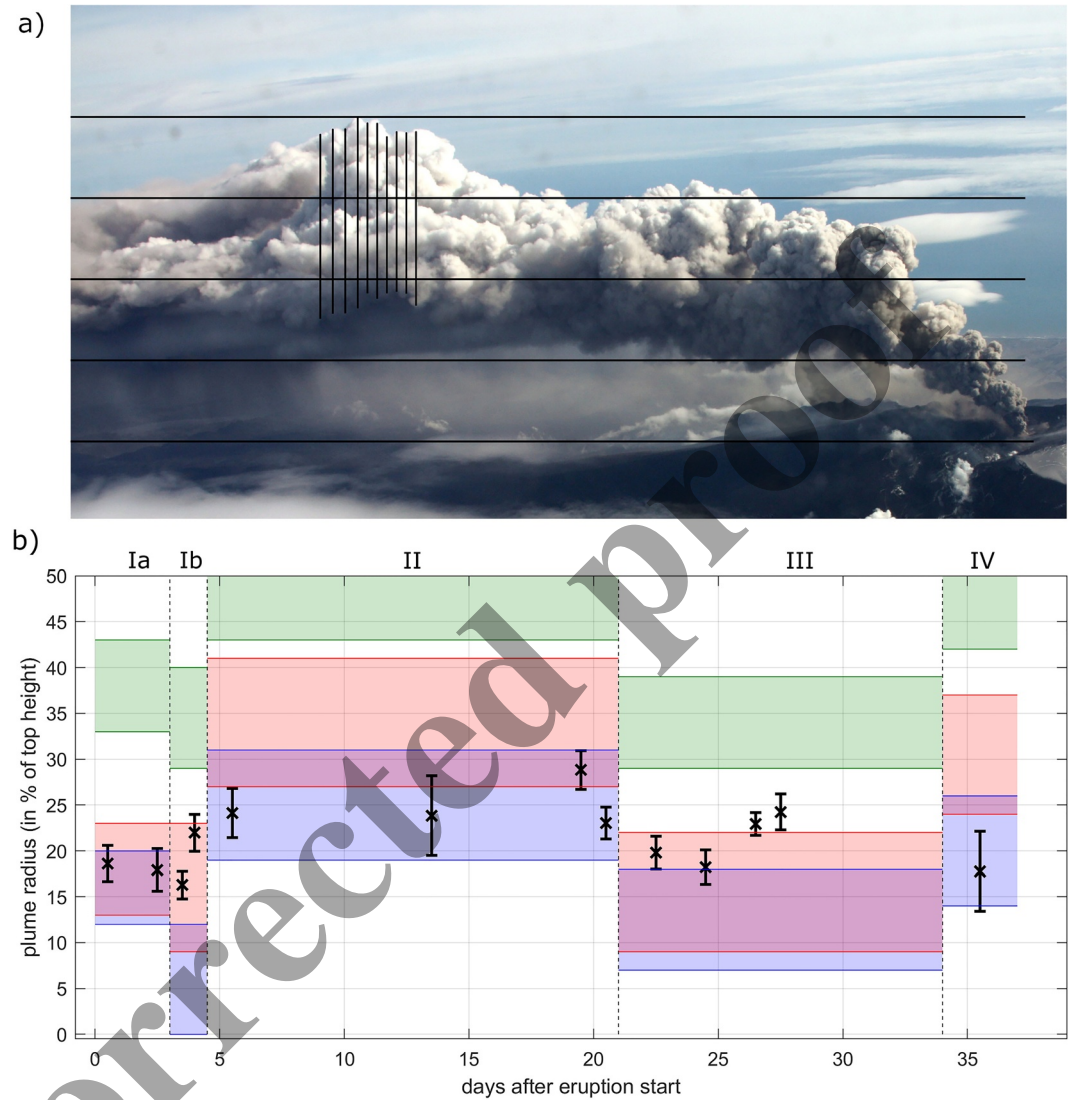


Figure 5. Plume radii of a weak plume. (a) Example of how plume diameter D was measured. The photo is taken on 4 May 2010, (eruption day 21) at 17:00 UTC. The plume's top height h was photogrammetrically determined to be ~ 5 km above vent, the distance between the horizontal lines is 1,250 m. Vertical lines mark the measured diameters. (b) Observed day-averaged normalized plume radii r_{obs} (black markers) are compared with the predicted ranges of r , computed with the WM (blue), the DBM with $\beta = 0.5$ (green) and the DBM with $\beta = 0.33$ (red). Ranges of modeled plume radii reflect the uncertainties of M_{ground} . Error bars of r_{obs} are computed by using the standard deviations of each point.

(Figure 6c). This leads to broad ranges of “possible” a -values (see also Table 3) and provides larger flexibility to fit the model to observations, compared to the r -strategy. In Figure 6, the observed ranges of normalized plume radii r_{obs} are indicated by red dashed lines. While the WM underestimates the MER for phases Ib and III when using r_{obs} in conjunction with the r -strategy, it is now possible for any phase to use r_{obs} values for a and constrain the complementary correction factor b (see Figure 6, Table 3) to obtain more accurate estimates.

Fitting the normalized observed plume radii r_{obs} and measured masses M_{ground} to the predictions from the DBM is not possible with a β of 0.50 (see Figure 6g, Table 3). Only with reduced wind entrainment rates ($0.28 \leq \beta \leq 0.36$) the (a, b) corridor lies within the observed range (Figures 6h and 6i).

3.4. Effect of Other Model Parameters on MER

So far, we kept the model parameters other than β fixed. Since the source temperature T_0 and the specific heat capacity of the mixture C are not exactly known, we tested the robustness of our findings toward variation of these

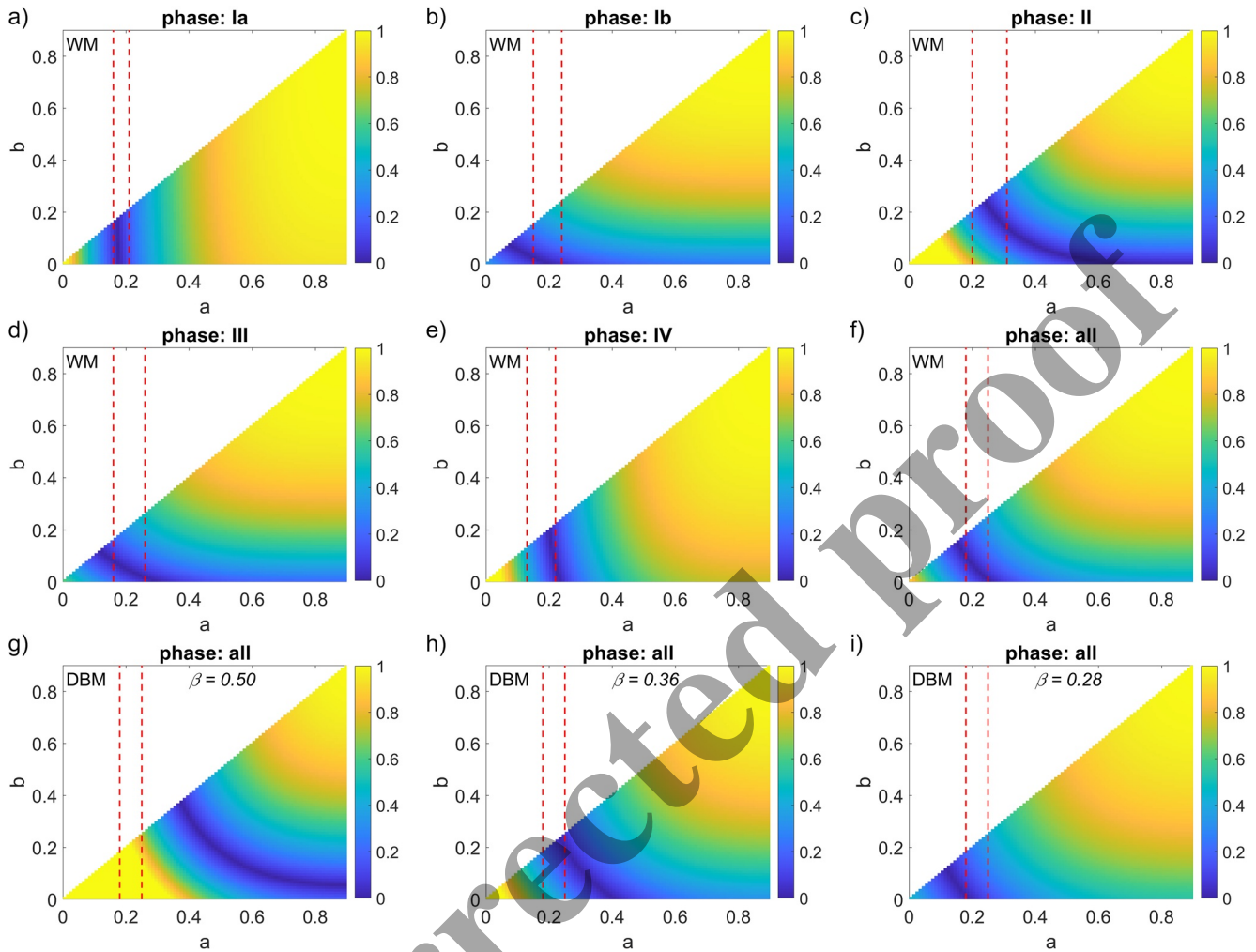


Figure 6. Results for correction factors a and b according to the ab -strategy. Coloration of a pixel indicates the absolute value of the difference between the modeled mass M_{model} and measured mass M_{ground} , normalized with respect to M_{ground} , when using H_v according to Equations 11 and 12 with the corresponding values for a and b . Dark blue color indicates combinations (a, b) , for which model predictions fit best with the measured mass eruption rate. The ranges of normalized observed plume radii r_{obs} are marked by red dashed lines. In panels (a–e) the phase-specific results obtained by the WM (Woodhouse et al., 2013) are shown. Panel (f) represents the result with the WM for the complete Eyjafjallajökull 2010 eruption (“all”). In the bottom row, the corresponding (a, b) results for the DBM (Degruyter & Bonadonna, 2012) are displayed (g) for $\beta = 0.50$, (h) $\beta = 0.36$, and (i) $\beta = 0.28$. The latter two values define the range of β , for which a and r_{obs} overlap most.

parameters. Within the assumed uncertainty range of 150 K for T_0 , the MER predicted by the DBM for a 5 km high plume changes by less than 2%, and the values for r_{DBM} found with the r -strategy vary by less than 4%. The range of β obtained with the ab -strategy shifts slightly by ± 0.03 . It would require a 1000°C hotter source (thus an unrealistic T_0 of 2223 K) to find an overlap of r_{DBM} with r_{obs} , or to find a solution with the DBM and ab -strategy that fit the observations.

A variation of C_0 of by $\pm 200 \text{ J kg}^{-1} \text{ K}^{-1}$ causes only minor changes (less than 4%) in the resulting range for r_{DBM} . It would require $\pm 300 \text{ J kg}^{-1} \text{ K}^{-1}$ to shift the range for r_{DBM} by 5%. To find any solution for a and b with the DBM and $\beta = 0.50$, C_0 would need to be assigned an unrealistic value of 2,250 $\text{J kg}^{-1} \text{ K}^{-1}$ or larger. Under variation of Π_i by ± 0.01 , M_{model} would change by less than 6%. We therefore conclude that the presented results are robust for the ranges of $T_0 \pm 150 \text{ K}$, $C_0 \pm 300 \text{ J kg}^{-1} \text{ K}^{-1}$ and $\Pi_i \pm 0.01$.

We note that the heat capacity of the plume also depends on the humidity of the column, which varies between the phreatomagmatic and the dry phases (Degruyter & Bonadonna, 2012). Furthermore, phreatomagmatic eruptions are known to produce finer ash (Dürig et al., 2020; Zimanowski et al., 2003), which changes the density of the plume mixture. Both effects might have implicitly affected the results for r , b , and β , when comparing

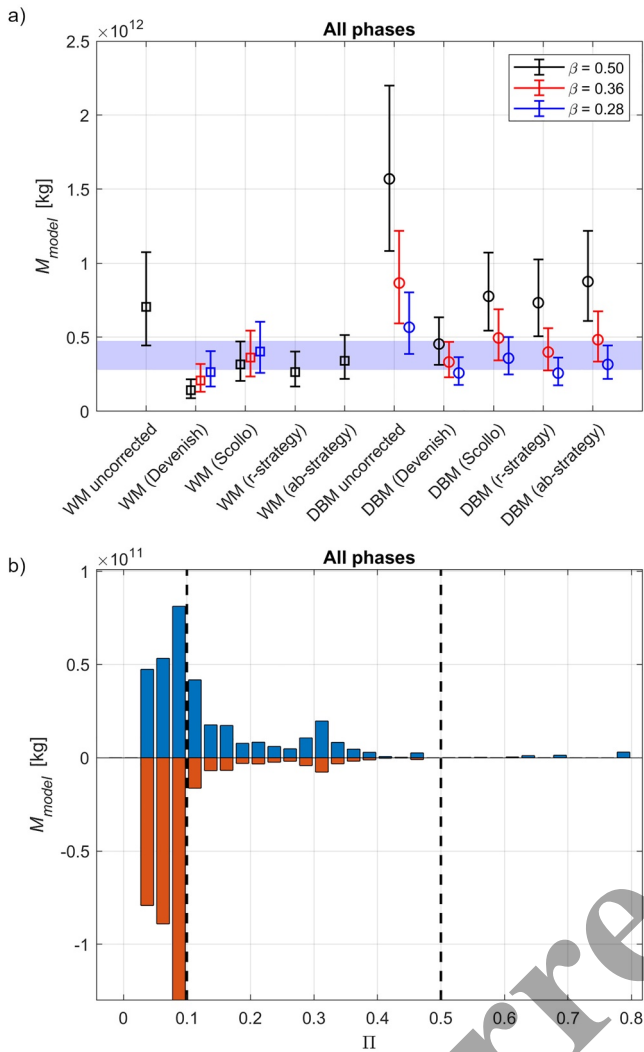


Figure 7. Impact of centerline-correction strategies on M_{model} . (a) Uncorrected model predictions and estimates based on different centerline correction strategies are compared with the range of fallout mass M_{ground} (highlighted in violet shade). Values used were: $r = 0.22$, $a = 0.22$, $b = 0.8$. (b) Blue bars in this histogram show M_{model} computed with WM and *ab*-strategy using $a = 0.22$ and $b = 0.08$, binned by Π -values. Red bars show the mass that was subtracted from the original (uncorrected) mass. Vertical dashed lines separate weak, intermediate and strong plume regimes.

the phreatomagmatic phase I with the predominantly dry phases II–IV. They cannot, however, explain why the variation of these parameters within phase I (Ia vs. Ib) is of the same order of magnitude as between dry and wet phases (see Figure 5b). While certainly being an important aspect to be studied in the future, our findings for Eyjafjallajökull 2010 indicate that it is the effect of wind on the plume, which dominantly controls the quality of the model prediction.

3.5. Comparison With Theoretical Centerline-Correction Approaches

The uncorrected estimates by WM and DBM for the complete Eyjafjallajökull 2010 eruption are shown in Figure 7a, together with M_{model} results based on the different centerline-correction strategies tested. Since at any point in time of the eruption $\bar{v} > 20$, for Eyjafjallajökull 2010 the correction by Devenish (2016) coincides with the *r*-strategy, but it uses r_{Dev} instead of r_{obs} . According to Equation 14, for $\beta = 0.50$ the normalized plume radius r_{Dev} is estimated to be $\sim 33\%$, which is larger than the observed range of 18%–25%. Consequently, a correction with the Devenish-strategy and $\beta = 0.50$ results in an underestimation of the mass modeled by WM (M_{WM}). When using r_{obs} in combination with Equation 14 and solving it for β , we obtain:

$$\beta_{\text{obs}} = \frac{r_{\text{obs}}}{(1 - r_{\text{obs}})} \quad (15)$$

with which we can estimate the wind entrainment rates β_{obs} for which the theoretical normalized plume radii match the observations, that is, $r_{\text{Dev}} = r_{\text{obs}}$. For $18\% \leq r_{\text{obs}} \leq 25\%$, this is fulfilled for $0.22 \leq \beta_{\text{obs}} \leq 0.33$, a range that agrees well with the estimates found by the *r*-strategy ($0.24 \leq \beta \leq 0.37$) and the *ab*-strategy ($0.28 \leq \beta \leq 0.36$). Choosing the latter values for β leads to clear improvement of WM's prediction quality (see Figure 7a). Without centerline-correction, M_{model} estimated by DBM (M_{DBM}) with $\beta = 0.50$ overestimates the erupted mass by more than 400%, which is more than twice the overestimate for the uncorrected M_{WM} ($\sim 190\%$). Consequently, it requires also a much larger correction. This might explain why a correction with the Devenish-strategy and $\beta = 0.50$ match similarly well with M_{ground} , as one with $\beta = 0.36$.

For the Scollo-strategy, reducing β from 0.50 to the range suggested by the *ab*-strategy improves the prediction quality of both models tested, although the differences are relatively small for the WM. The Scollo-strategy corrects only for $\Pi < 0.1$. Therefore, the results displayed in Figure 7a can also be regarded as results from an *ab*-strategy using $b = 0$ and $a = 0.33$, ~ 0.265 , and 0.22 (corresponding to $\beta = 0.50$, 0.36, and 0.28), respectively.

Figure 7a also shows the results for applying the *r*-strategy with $r = 0.22$ and for the *ab*-strategy with $a = 0.22$ and $b = 0.08$. The value of 0.22 represents the average observed normalized plume radius r_{obs} (see Table 3). The reasoning behind b is explained in the sections below. In summary, the observation-based *r*-strategy and *ab*-strategy and the theoretical Scollo-strategy work similarly well for the WM, and only the Devenish-strategy requires an adjustment of β . The prediction quality of the DBM, however, depends for all correction strategies on the choice of β . Our findings indicate that for Eyjafjallajökull 2010 the wind entrainment coefficient was significantly lower than 0.50, being rather in the range of $0.28 \leq \beta \leq 0.36$. For these lower wind entrainment coefficients, all tested centerline-correction strategies lead to estimates M_{model} that agree well with M_{ground} .

4. Discussion

The 2010 Eyjafjallajökull eruption was characterized by a quite complex and time-varying interaction between source and atmospheric conditions. The plume in phase Ia was dominantly weak, despite the fact that this

phreatomagmatic episode was the one featuring the largest MERs (see Table 2). Conversely, the MER was lowest for phase II, a phase of very low ash production. Yet, the Π -values suggest that this was the only phase where the plume was more often intermediate than weak. This demonstrates that for this eruption, the windspeed was the dominant factor for how the plume ascended, and was more influential than the MER. While during the strongest eruptive phase Ia windspeeds of up to ~ 60 m/s occurred at plume top altitude (Dürig, Gudmundsson, Ágústsdóttir, et al., 2022), wind velocities subsequently decreased. Phase II was the episode of the lowest average windspeeds with 11.8 m/s (Table 2). The Eyjafjallajökull 2010 eruption is therefore a good example of the ambiguity inherent in using the term “weak” for a bent-over plume and “strong” for a vertically rising plume. This ambiguity could be avoided by adopting alternative terms for the different plume types, such as “wind-dominated,” “intermediate,” and “buoyancy-dominated.”

Using the Π parameter with thresholds suggested by Scollo et al. (2019) has led to the plausible result that the Eyjafjallajökull plume was, with the exception of very few and short time intervals, wind-dominated or intermediate. Provided that a model delivers accurate predictions, it is to be expected that the r -strategy works best for a phase that is dominantly wind-dominated (where $r = r_{\text{obs}}$). This is approximately the case in phase Ia (94.5% “wind-dominated”) and phase IV (84.3% “wind-dominated”), for which the WM provides results that fit well with the observations. Following the r -strategy, the WM shows also good agreement with the observations for phase II, despite the fact that this phase had long episodes of intermediate plumes (45.7% “wind-dominated,” 53.1% “intermediate”). In contrast, the WM predictions do not fit well with the observations for phases Ib (62.0% “wind-dominated”) and III (58.6% “wind-dominated”). We therefore infer that for the WM, the r -strategy works best for plumes that are predominantly (i.e., for more than $\sim 85\%$ of the time) wind-dominated or for plumes subjected to relatively low windspeeds (< 12 m/s).

The above analysis indicates that the range of applicability for the r -strategy is quite limited. However, the ab -strategy appears to be a more widely applicable approach for converting observed plume heights into H_c that lead to accurate WAM predictions. A source of complication, however, is that this strategy requires the specification of a second parameter (the correction factor b). The optimal range of b for each phase, when using r_{obs} for a , is given in Table 3. Our results for Eyjafjallajökull 2010 suggest that in case of the WM, the optimal choice of b is $3\% = b \leq 13\%$ (which is why we used 0.08 for b in Figure 7a). For these values, b_{WM} overlaps for all eruptive phases (see row 8 in Table 3). The findings for the DBM do not provide such multi-phase overlaps for b , which makes it more challenging to apply the ab -strategy with this model.

Figure 7a demonstrates that to obtain an accurate estimate of H_c , the selection of β is significantly more important than the choice of b . This raises the question if and how intermediate plumes should be corrected, and if the ab -strategy with $a = r_{\text{obs}}$ could be simplified, for example, by using it always with $b = 0$ (applying no correction for intermediate plumes, similar to the Scollo-strategy) or with $b = a$ (applying the same correction for both wind-dominated and intermediate plumes). The blue bars in the histogram displayed in Figure 7b show M_{WM} after applying the ab -strategy with $a = 0.22$ (the mean value of r_{obs}) and $b = 0.08$, binned by Π . The red bars show the mass that was subtracted by this strategy, sorted by Π . In the depicted case, 84% of the subtracted mass can be attributed to a wind-dominated plume. During the complete Eyjafjallajökull 2010 eruption, 27% of the mass delivered under intermediate plume conditions falls in the bin closest to Π_i and the median is at $\Pi = 0.175$, much closer to the boundary of the wind-dominated than to that of the buoyancy-dominated regime. For such a scenario, it would be plausible if a correction for intermediate plume is required, and we would expect a notable difference between approaches that apply a correction for intermediate plumes (ab -strategy with $b \neq 0$), and those which don't (ab -strategy with $b = 0$). To further study the impact of the choice of b , we computed M_{model} for the WM and the DBM by applying ab -strategies with $a = 0.22$ while varying b for the complete eruption (Figure 8a) as well as for individual eruptive phases (three examples are shown in Figures 8b–8d). For the WM, β was kept constant (0.9), while for the DBM β was varied between 0.16 and 0.36. We group the eruptive phases in three categories:

1. For phases that were characterized by a predominantly wind-affected plume (Ia: 95% of total duration, IV: 84%, see Table 2), the impact of b is only marginal and barely changes the results, as demonstrated for phase IV in Figure 8d. For example, M_{model} from the WM overlaps with M_{ground} for all values of b .
2. Episodes which feature a plume that is for most of the time wind-affected, but is also characterized by considerable intermediate plume episodes, are the phases Ib (62%:38%), III (59%:40%) and the complete eruption (“all”; 59%:40%). While for the WM the optimal choice for b was found to be 0.08 when looking at the overall

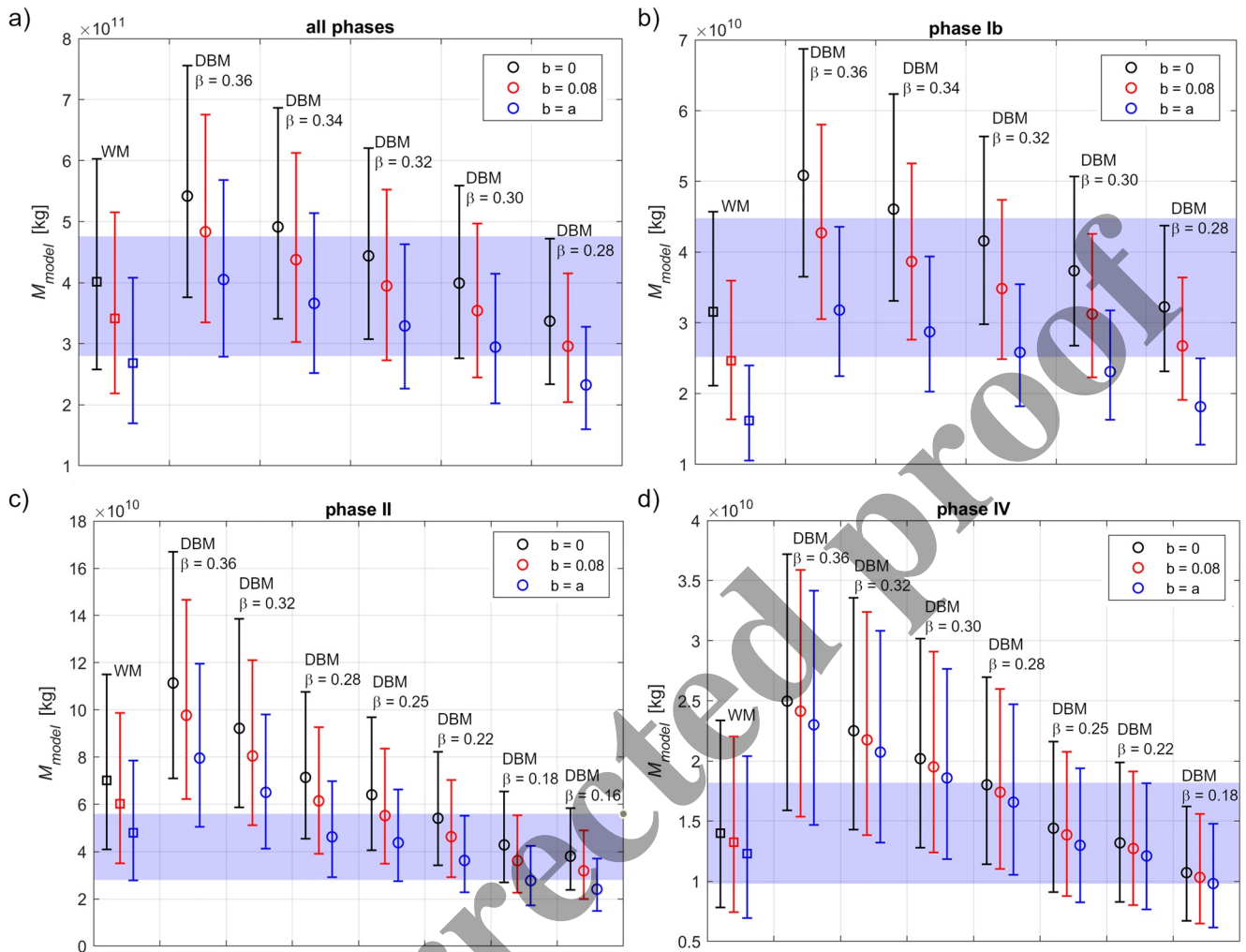


Figure 8. Results for M_{model} for the indicated eruption phases after applying the ab -strategy with various settings for β , a , and b . The measured range for M_{ground} is marked in violet shade.

eruption and phase III, this does not apply for phase Ib. There, using $b \neq 0$ does not improve the correction quality of the ab -strategy on the WM. In contrast, for all phases of this category the predictions from the DBM can be optimized by an adjustment of b within the suggested range of β . Using $b = 0$ and $\beta = 0.28$ leads to an estimate that is in good agreement with M_{ground} , but to an overestimate of the modeled erupted mass when using $\beta = 0.36$. In contrast, choosing a large value for b ($b \approx a$) leads to matching results for $\beta = 0.36$, but to an overcorrection of mass for $\beta = 0.28$. It was found that using $b = 0.08$, as for the WM, is also a good compromise for the DBM, since it leads to predictions that overlap with the observations for most values of β that lie in the range suggested by the findings with the ab -strategy (Figures 8a and 8b). We note that the ratio between $b = 0.08$ and $a = 0.22$ is approximately 40:60, a proportion which coincides with that of the periods of intermediate versus wind-dominated plumes. It would require, however, a larger data set from different eruptions, to find out if this is more than a coincidence.

- Phase II was the only eruptive phase of Eyjafjallajökull 2010 in which the plume was intermediate over longer periods than it was wind-dominated (53% vs. 46%). For this phase, predictions from the WM fit best when using $b = a$ (Figure 8c), which is the maximum possible value for b . If we limit the range of β to the constraints found earlier (i.e., $0.28 = \beta \leq 0.36$) the same solution for b is also found for the DBM. We note, however, that this high value for b might also indicate that β was, in fact, smaller than the suggested range.

All results from the centerline-correction strategies examined consistently indicate that the DBM simulates the Eyjafjallajökull 2010 eruption best by using a wind entrainment coefficient $0.28 = \beta \leq 0.36$. We have also

demonstrated that using Equation 15 with observational data of the plume radius give very similar results. The values found for β are lower than suggested in most studies (e.g., Bursik, 2001; Degruyter & Bonadonna, 2012, 2013; Michaud-Dubuy et al., 2020), but in good agreement with the work by Suzuki and Koyaguchi (2015), who suggested β to range between 0.1 and 0.3, based on numerical simulations and on observations for the 2011 Shinmoe-dake eruption, which featured a predominantly wind-affected plume. One possible conclusion from this mismatch might be that β should not be treated as a universal constant, but as a variable that depends on the eruptive conditions (Carazzo et al., 2014) and that has to be determined specifically for each eruptive scenario and plume model.

5. Conclusions and Outlook

The present study reveals that when using plume heights as the principal input, the tested explicitly WAMs of MERs require adjusted plume heights H_c as input, not the directly observable plume top elevation h . In this study, we introduced and explored two strategies for using plume radius observations to convert h into H_c . We used empirical data from the Eyjafjallajökull 2010 eruption to test the centerline-correction strategies by applying them to two WAMs and compared the results with those obtained from two theoretical correction approaches introduced by Devenish (2016) and by Scollo et al. (2019).

It turned out that the optimal plume height treatment strategy for the Woodhouse plume model (Woodhouse et al., 2013) is to use Π introduced by Degruyter and Bonadonna (2012) with the thresholds 0.1 and 0.5 as suggested by Scollo et al. (2019) to distinguish between three plume-types. H_c is computed according to the *ab*-strategy, defined by Equations 10–12, using the observed normalized plume radius r_{obs} for a , together with the correction factor b . The latter parameter depends on the dominant plume type of the observed eruption. According to our findings for Eyjafjallajökull 2010, phases in which the plume was predominantly wind-affected (>80% of the time) are best corrected with $b = 0$. Phases with mostly wind-dominated but also considerable intermediate plume episodes (with the ratio ~60:40) are best corrected with $b = 0.08$, which in respect to a represents roughly the ratio of plume types observed. Within the suggested range of β , for the only phase of Eyjafjallajökull 2010 that featured a mostly intermediate plume, the optimal correction strategy is the *ab*-strategy with $b = a$.

Although the number of plume radii observations for Eyjafjallajökull 2010 is based on only 31 snapshots and thus relatively low given the long total duration of this eruption, we have demonstrated how our approach can also be used to constrain the wind entrainment coefficient β , based on empirical eruptive data. Constraining this parameter is crucial for the strategies discussed. Our findings from modeling Eyjafjallajökull 2010 with the plume model of Degruyter and Bonadonna (2012) consistently indicate that β ranges for this eruption between 0.28 and 0.36, which is smaller than used in most previous studies.

While more sophisticated ways exist to accurately constrain β , for example, with laboratory experiments (Carazzo et al., 2014; Michaud-Dubuy et al., 2020), experimental laws linking β to the local buoyancy conditions quantified by the Richardson number (Tate, 2002) or with complex numerical models to simulate observations (Suzuki & Koyaguchi, 2015), we found that, at least for Eyjafjallajökull 2010, the wind entrainment coefficient can be approximated by using r_{obs} from plume observations in combination with a simple relationship, given by Equation 15. With the possibility to assess β , the *ab*-strategy could be applied semi-automatically, for example, in combination with the real-time monitoring software REFIR, which would lead to more accurate predictions for eruptions with wind-affected plumes. To test if the findings from Eyjafjallajökull 2010 apply unchanged to other eruptions, it is, however, necessary to apply the methodology presented to a wider range of eruptive data sets under a variety of wind conditions.

Conflict of Interest

The authors declare no conflicts of interest relevant to this study.

Data Availability Statement

All data to understand, evaluate, and build upon the research reported in this manuscript can be downloaded from <https://doi.org/10.5281/zenodo.7040203> (Dürig, Gudmundsson, Dioguardi, & Schmidt, 2022).

Acknowledgments

The authors thank Þórhólfur Högnadóttir for compiling Figure 2 and Larry Mastin as well as four anonymous reviewers for their helpful comments. TD was supported by the Icelandic Research Fund (Rannís) post-doctoral project Grant 206527-051. This work is published with permission of the Executive Director of British Geological Survey (UKRI).

References

- Arason, P., Petersen, G. N., & Björnsson, H. (2011). Observations of the altitude of the volcanic plume during the eruption of Eyjafjallajökull, April–May 2010. *Earth System Science Data*, 3(1), 9–17. <https://doi.org/10.5194/essd-3-9-2011>
- Blake, D., Wilson, T., Cole, J., Deligne, N., & Lindsay, J. (2017). Impact of volcanic ash on road and airfield surface skid resistance. *Sustainability*, 9(8), 1389. <https://doi.org/10.3390/su9081389>
- Blong, R. J., Grasso, P., Jenkins, S. F., Magill, C. R., Wilson, T. M., McMullan, K., & Kandlbauer, J. (2017). Estimating building vulnerability to volcanic ash fall for insurance and other purposes. *Journal of Applied Volcanology*, 6(1), 2. <https://doi.org/10.1186/s13617-017-0054-9>
- Bonadonna, C., Cioni, R., Costa, A., Drürit, T., Phillips, J., Pioli, L., et al. (2016). MeMoVolc report on classification and dynamics of volcanic explosive eruptions. *Bulletin of Volcanology*, 78(11), 84. <https://doi.org/10.1007/s00445-016-1071-y>
- Bonadonna, C., Pistolesi, M., Cioni, R., Degruyter, W., Elissondo, M., & Baumann, V. (2015). Dynamics of wind-affected volcanic plumes: The example of the 2011 Cordón Caulle eruption, Chile. *Journal of Geophysical Research: Solid Earth*, 120(4), 2242–2261. <https://doi.org/10.1002/2014JB011478>
- Bursik, M. (2001). Effect of wind on the rise height of volcanic plumes. *Geophysical Research Letters*, 28(18), 3621–3624. <https://doi.org/10.1029/2001GL013393>
- Carazzo, G., Girault, F., Aubry, T., Bouquerel, H., & Kaminski, E. (2014). Laboratory experiments of forced plumes in a density-stratified crossflow and implications for volcanic plumes. *Geophysical Research Letters*, 41(24), 8759–8766. <https://doi.org/10.1002/2014GL061887>
- Carazzo, G., Kaminski, E., & Tait, S. (2006). The route to self-similarity in turbulent jets and plumes. *Journal of Fluid Mechanics*, 547(1), 137. <https://doi.org/10.1017/S002211200500683X>
- Carey, S., & Sparks, R. S. J. (1986). Quantitative models of the fallout and dispersal of tephra from volcanic eruption columns. *Bulletin of Volcanology*, 48(2–3), 109–125. <https://doi.org/10.1007/BF01046546>
- Contini, D., Donato, A., Cesari, D., & Robins, A. G. (2011). Comparison of plume rise models against water tank experimental data for neutral and stable cross flows. *Journal of Wind Engineering and Industrial Aerodynamics*, 99(5), 539–553. <https://doi.org/10.1016/j.jweia.2011.02.003>
- Costa, A., Suzuki, Y. J., Cerminara, M., Devenish, B. J., Ongaro, T. E., Herzog, M., et al. (2016). Results of the eruptive column model inter-comparison study. *Journal of Volcanology and Geothermal Research*, 326, 2–25. <https://doi.org/10.1016/j.jvolgeores.2016.01.017>
- Degruyter, W., & Bonadonna, C. (2012). Improving on mass flow rate estimates of volcanic eruptions. *Geophysical Research Letters*, 39(16), 1–6. <https://doi.org/10.1029/2012GL052566>
- Degruyter, W., & Bonadonna, C. (2013). Impact of wind on the condition for column collapse of volcanic plumes. *Earth and Planetary Science Letters*, 377–378, 218–226. <https://doi.org/10.1016/j.epsl.2013.06.041>
- Dellino, P., Dioguardi, F., Mele, D., D'Addabbo, M., Zimanowski, B., Büttner, R., et al. (2014). Volcanic jets, plumes, and collapsing fountains: Evidence from large-scale experiments, with particular emphasis on the entrainment rate. *Bulletin of Volcanology*, 76(6), 834. <https://doi.org/10.1007/s00445-014-0834-6>
- Dellino, P., Gudmundsson, M. T., Larsen, G., Mele, D., Stevenson, J. A., Thordarson, T., & Zimanowski, B. (2012). Ash from the Eyjafjallajökull eruption (Iceland): Fragmentation processes and aerodynamic behavior. *Journal of Geophysical Research*, 117(B9), B00C04. <https://doi.org/10.1029/2011JB008726>
- de' Michieli Vitturi, M., Neri, A., & Barsotti, S. (2015). PLUME-MoM 1.0: A new integral model of volcanic plumes based on the method of moments. *Geoscientific Model Development*, 8(8), 2447–2463. <https://doi.org/10.5194/gmd-8-2447-2015>
- Devenish, B. J. (2013). Using simple plume models to refine the source mass flux of volcanic eruptions according to atmospheric conditions. *Journal of Volcanology and Geothermal Research*, 256, 118–127. <https://doi.org/10.1016/j.jvolgeores.2013.02.015>
- Devenish, B. J. (2016). Estimating the total mass emitted by the eruption of Eyjafjallajökull in 2010 using plume-rise models. *Journal of Volcanology and Geothermal Research*, 326, 114–119. <https://doi.org/10.1016/j.jvolgeores.2016.01.005>
- Dioguardi, F., Beckett, F., Dürig, T., & Stevenson, J. A. (2020). The impact of eruption source parameter uncertainties on ash dispersion forecasts during explosive volcanic eruptions. *Journal of Geophysical Research: Atmospheres*, 125(17), e2020JD032717. <https://doi.org/10.1029/2020JD032717>
- Dioguardi, F., Dürig, T., Engwell, S. L., Gudmundsson, M. T., & Loughlin, S. C. (2016). Investigating source conditions and controlling parameters of explosive eruptions: Some experimental-observational-modelling case studies. In K. Németh (Ed.), *Updates in volcanology – From volcano modelling to volcano geology*. InTech. <https://doi.org/10.5772/63422>
- Dürig, T., Gudmundsson, M. T., Ágústadóttir, T., Högnadóttir, T., & Schmidt, L. S. (2022). The effect of wind and plume height reconstruction methods on the accuracy of simple plume models — A second look at the 2010 Eyjafjallajökull eruption. *Bulletin of Volcanology*, 84(3), 33. <https://doi.org/10.1007/s00445-022-01541-z>
- Dürig, T., Gudmundsson, M. T., & Dellino, P. (2015). Reconstruction of the geometry of volcanic vents by trajectory tracking of fast ejecta – The case of the Eyjafjallajökull 2010 eruption (Iceland). *Earth Planets and Space*, 67(1), 64. <https://doi.org/10.1186/s40623-015-0243-x>
- Dürig, T., Gudmundsson, M. T., Dioguardi, F., & Schmidt, L. S. (2022). Data depositor – “Quantifying the effect of wind on volcanic plumes: Implications for plume modelling” [Dataset]. Zenodo. <https://doi.org/10.5281/zenodo.7040203>
- Dürig, T., Gudmundsson, M. T., Dioguardi, F., Woodhouse, M., Björnsson, H., Barsotti, S., et al. (2018). REFIR – A multi-parameter system for near real-time estimates of plume-height and mass eruption rate during explosive eruptions. *Journal of Volcanology and Geothermal Research*, 360, 61–83. <https://doi.org/10.1016/j.jvolgeores.2018.07.003>
- Dürig, T., Gudmundsson, M. T., Karmann, S., Zimanowski, B., Dellino, P., Rietze, M., & Büttner, R. (2015). Mass eruption rates in pulsating eruptions estimated from video analysis of the gas thrust-buoyancy transition—A case study of the 2010 eruption of Eyjafjallajökull, Iceland. *Earth Planets and Space*, 67(1), 180. <https://doi.org/10.1186/s40623-015-0351-7>
- Dürig, T., White, J. D. L., Murch, A. P., Zimanowski, B., Büttner, R., Mele, D., et al. (2020). Deep-sea eruptions boosted by induced fuel-coolant explosions. *Nature Geoscience*, 13(7), 498–503. <https://doi.org/10.1038/s41561-020-0603-4>
- Folch, A., Costa, A., & Macedonio, G. (2016). FPLUME-1.0: An integral volcanic plume model accounting for ash aggregation. *Geoscientific Model Development*, 9(1), 431–450. <https://doi.org/10.5194/gmd-9-431-2016>
- Giehl, C., Brooker, R. A., Marxer, H., & Nowak, M. (2017). An experimental simulation of volcanic ash deposition in gas turbines and implications for jet engine safety. *Chemical Geology*, 461, 160–170. <https://doi.org/10.1016/j.chemgeo.2016.11.024>
- Grindle, T. J., & Burcham, F. W. (2002). Even minor volcanic ash encounters can cause major damage to aircraft. *JCAO Journal*, 57(29), 12–14.
- Gudmundsson, M. T., Thordarson, T., Hoskuldsson, A., Larsen, G., Björnsson, H., Prata, F. J., et al. (2012). Ash generation and distribution from the April–May 2010 eruption of Eyjafjallajökull, Iceland. *Scientific Reports*, 2, 1–12. <https://doi.org/10.1038/srep00572>
- Hersbach, H., Bell, B., Berrisford, P., Biavati, G., Horányi, A., Muñoz Sabater, J., et al. (2018). ERA5: Fifth generation of ECMWF atmospheric reanalyses of the global climate. Copernicus Climate Change Service Climate Data Store (CDS).

- Hersbach, H., Bell, B., Berrisford, P., Hirahara, S., Horányi, A., Muñoz-Sabater, J., et al. (2020). The ERA5 global reanalysis. *Quarterly Journal of the Royal Meteorological Society*, 146(730), 1999–2049. <https://doi.org/10.1002/qj.3803>
- Hewett, T. A., Fay, J. A., & Hault, D. P. (1971). Laboratory experiments of smokestack plumes in a stable atmosphere. *Atmospheric Environment*, 5(9), 767–789. [https://doi.org/10.1016/0004-6981\(71\)90028-X](https://doi.org/10.1016/0004-6981(71)90028-X)
- Hochfeld, I., Hort, M., Schwalbe, E., & Dürig, T. (2022). Eruption dynamics of Anak Krakatau volcano (Indonesia) estimated using photogrammetric methods. *Bulletin of Volcanology*, 84(8), 73. <https://doi.org/10.1007/s00445-022-01579-z>
- Huq, P., & Stewart, E. J. (1996). A laboratory study of buoyant plumes in laminar and turbulent crossflows. *Atmospheric Environment*, 30(7), 1125–1135. [https://doi.org/10.1016/1352-2310\(95\)00335-5](https://doi.org/10.1016/1352-2310(95)00335-5)
- Jenkins, S. F., Wilson, T. M., Magill, C., Miller, V., Stewart, C., Blong, R., et al. (2015). Volcanic ash fall hazard and risk. In S. C. Loughlin, S. Sparks, S. K. Brown, S. F. Jenkins, & C. Vye-Brown (Eds.), *Global volcanic hazards and risk* (pp. 173–222). Cambridge University Press. <https://doi.org/10.1017/CBO9781316276273.005>
- Keiding, J. K., & Sigmarsson, O. (2012). Geothermobarometry of the 2010 Eyjafjallajökull eruption: New constraints on Icelandic magma plumbing systems. *Journal of Geophysical Research*, 117(B9), B00C09. <https://doi.org/10.1029/2011JB008829>
- Londono, J. M., & Galvis, B. (2018). Seismic data, photographic images and physical modeling of volcanic plumes as a tool for monitoring the activity of Nevado del Ruiz Volcano, Colombia. *Frontiers of Earth Science*, 6(November), 162. <https://doi.org/10.3389/feart.2018.00162>
- Magnússon, R. L. (2012). *Pixelcalc: Forrit til mælinga á stærð gosmokka út frá stafrænum myndum (Pixelcalc: Software to measure height of eruption plumes from digital photos)*. University of Iceland. Retrieved from https://notendur.hi.is/mtg/pdf/RH-2012-08_pixelcalc-report.pdf
- Mastin, L. G. (2014). Testing the accuracy of a 1-D volcanic plume model in estimating mass eruption rate. *Journal of Geophysical Research: Atmospheres*, 119(5), 2474–2495. <https://doi.org/10.1002/2013JD020604>
- Mastin, L. G., Guffanti, M., Servranckx, R., Webley, P., Barsotti, S., Dean, K., et al. (2009). A multidisciplinary effort to assign realistic source parameters to models of volcanic ash-cloud transport and dispersion during eruptions. *Journal of Volcanology and Geothermal Research*, 186(1–2), 10–21. <https://doi.org/10.1016/j.jvolgeores.2009.01.008>
- Michaud-Dubuy, A., Carazzo, G., & Kaminski, E. (2020). Wind entrainment in jets with reversing Buoyancy: Implications for volcanic plumes. *Journal of Geophysical Research: Solid Earth*, 125(10), 1–18. <https://doi.org/10.1029/2020JB020136>
- Morton, B. R., Taylor, G., & Turner, J. S. (1956). Turbulent gravitational convection from maintained and instantaneous sources. *Proceedings of the Royal Society of London, Series A: Mathematical and Physical Sciences*, 234(1196), 1–23. <https://doi.org/10.1098/rspa.1956.0011>
- Nawri, N., Pálmason, B., Petersen, N. G., Björnsson, H., & Þorsteinsson, S. (2017). *The ICRA atmospheric reanalysis project for Iceland* (Report VÍ 2017-005, pp. 37). Icelandic Met Office. Retrieved from http://www.vedur.is/media/vedurstofan-utgafa-2017/VI_2017_005_rs.pdf
- Papanicolaou, P. N., Papakonstantis, I. G., & Christodoulou, G. C. (2008). On the entrainment coefficient in negatively buoyant jets. *Journal of Fluid Mechanics*, 614, 447–470. <https://doi.org/10.1017/S0022112008003509>
- Ripepe, M., Bonadonna, C., Folch, A., Delle Donne, D., Lacanna, G., Marchetti, E., & Höskuldsson, A. (2013). Ash-plume dynamics and eruption source parameters by infrasound and thermal imagery: The 2010 Eyjafjallajökull eruption. *Earth and Planetary Science Letters*, 366, 112–121. <https://doi.org/10.1016/j.epsl.2013.02.005>
- Rossi, E., Bonadonna, C., & Degruyter, W. (2019). A new strategy for the estimation of plume height from clast dispersal in various atmospheric and eruptive conditions. *Earth and Planetary Science Letters*, 505, 1–12. <https://doi.org/10.1016/j.epsl.2018.10.007>
- Schmidt, L., Langen, P., Aðalgeirsdóttir, G., Pálsson, F., Guðmundsson, S., & Gunnarsson, A. (2018). Sensitivity of Glacier runoff to winter snow thickness investigated for Vatnajökull ice cap, Iceland, using numerical models and observations. *Atmosphere*, 9(11), 450. <https://doi.org/10.3390/atmos9110450>
- Scollo, S., Prestifilippo, M., Bonadonna, C., Cioni, R., Corradini, S., Degruyter, W., et al. (2019). Near-real-time tephra fallout assessment at Mt. Etna, Italy. *Remote Sensing*, 11(24), 2987. <https://doi.org/10.3390/rs11242987>
- Scollo, S., Prestifilippo, M., Pecora, E., Corradini, S., Merucci, L., Spata, G., & Coltelli, M. (2014). Eruption column height estimation of the 2011–2013 Etna lava fountains. *Annals of Geophysics*, 57(2), S0214. <https://doi.org/10.4401/ag-6396>
- Sparks, R. S. J., Bursik, M. I., Carey, S. N., Gilbert, J. S., Glaze, L. S., Sigurdsson, H., & Woods, A. W. (1997). *Volcanic plumes*. John Wiley & Sons.
- Suzuki, Y. J., & Koyaguchi, T. (2015). Effects of wind on entrainment efficiency in volcanic plumes. *Journal of Geophysical Research: Solid Earth*, 120(9), 6122–6140. <https://doi.org/10.1002/2015JB012208>
- Tate, P. M. (2002). *The rise and dilution of buoyant jets and their behaviour in an internal wave field* (PhD thesis, pp. 220). University of New South Wales. <https://doi.org/10.26190/unsworks/21227>
- Turner, J. S. (1986). Turbulent entrainment: The development of the entrainment assumption, and its application to geophysical flows. *Journal of Fluid Mechanics*, 173, 431–471. <https://doi.org/10.1017/S0022112086001222>
- Wilson, L., & Walker, G. P. L. (1987). Explosive volcanic eruptions – VI. Ejecta dispersal in Plinian eruptions: The control of eruption conditions and atmospheric properties. *Geophysical Journal International*, 89(2), 657–679. <https://doi.org/10.1111/j.1365-246X.1987.tb05186.x>
- Woodhouse, M. J., Hogg, A. J., Phillips, J. C., & Sparks, R. S. J. (2013). Interaction between volcanic plumes and wind during the 2010 Eyjafjallajökull eruption, Iceland. *Journal of Geophysical Research: Solid Earth*, 118(1), 92–109. <https://doi.org/10.1029/2012JB009592>
- Woods, A. W. (1988). The fluid dynamics and thermodynamics of eruption columns. *Bulletin of Volcanology*, 50(3), 169–193. <https://doi.org/10.1007/BF01079681>
- Zimanowski, B., Wohletz, K., Dellino, P., & Büttner, R. (2003). The volcanic ash problem. *Journal of Volcanology and Geothermal Research*, 122(1–2), 1–5. [https://doi.org/10.1016/s0377-0273\(02\)00471-7](https://doi.org/10.1016/s0377-0273(02)00471-7)